Chapter 8

The Ekman Layer

ABSTRACT
Frictional forces, neglected in the previous chapter, are now investigated. Their main effect is to create horizontal boundary layers that support a flow transverse to the main flow of the fluid. The numerical treatment of the velocity profiles dominated by friction is illustrated with a spectral approach.

8.1 SHEAR TURBULENCE

Because most geophysical fluid systems are much shallower than they are wide, their vertical confinement forces the flow to be primarily horizontal. Unavoidable in such a situation is friction between the main horizontal motion and the bottom boundary. Friction acts to reduce the velocity in the vicinity of the bottom, thus creating a vertical shear. Mathematically, if u is the velocity component in one of the horizontal directions and z the elevation above the bottom, then u is a function of z, at least for small z values. The function $u(z)$ is called the *velocity profile* and its derivative $\mathrm{d}u/\mathrm{d}z$, the *velocity shear*.

Geophysical flows are invariably turbulent (high Reynolds number), and this greatly complicates the search for the velocity profile. As a consequence, much of what we know is derived from observations of actual flows, either in the laboratory or in the nature.

The turbulent nature of the shear flow along a flat or rough surface includes variability at short time and length scales, and the best observational techniques for the detailed measurements of these have been developed for the laboratory rather than outdoor situations. Laboratory measurements of nonrotating turbulent flows along smooth straight surfaces have led to the conclusion that the velocity varies solely with the stress τ_b exerted against the bottom, the fluid molecular viscosity ν, the fluid density ρ and, of course, the distance z above the bottom. Thus,

$$u(z) = F(\tau_b, \nu, \rho, z).$$

Introduction to Geophysical Fluid Dynamics, Volume 101, ISSN 0074-6142, DOI: 10.1016/B978-0-12-088759-0.00008-0

Dimensional analysis permits the elimination of the mass dimension shared by τ_b and ρ but not present in u, ν, and z, and we may write more simply:

$$u(z) = F\left(\frac{\tau_b}{\rho}, \nu, z\right).$$

The ratio τ_b/ρ has the same dimension as the square of a velocity, and for this reason, it is customary to define

$$u_* = \sqrt{\frac{\tau_b}{\rho}}, \tag{8.1}$$

which is called the *friction velocity* or *turbulent velocity*. Physically, its value is related to the orbital velocity of the vortices that create the cross-flow exchange of particles and the momentum transfer.

The velocity structure thus obeys a relation of the form $u(z) = F(u_*, \nu, z)$, and further use of dimensional analysis reduces it to a function of a single variable:

$$\frac{u(z)}{u_*} = F\left(\frac{u_* z}{\nu}\right). \tag{8.2}$$

In the presence of rotation, the Coriolis parameter enters the formalism, and the preceding function depends on two variables:

$$\frac{u(z)}{u_*} = F\left(\frac{u_* z}{\nu}, \frac{fz}{u_*}\right). \tag{8.3}$$

8.1.1 Logarithmic Profile

The observational determination of the function F in the absence of rotation has been repeated countless times, yielding the same results every time, and it suffices here to provide a single report (Fig. 8.1). When the velocity ratio u/u_* is plotted versus the logarithm of the dimensionless distance $u_* z/\nu$, not only do all the points coalesce onto a single curve, confirming that there is indeed no other variable to be invoked, but the curve also behaves as a straight line over a range of two orders of magnitude (from $u_* z/\nu$ between 10^1 and 10^3).

If the velocity is linearly dependent on the logarithm of the distance, then we can write for this portion of the velocity profile:

$$\frac{u(z)}{u_*} = A \ln \frac{u_* z}{\nu} + B.$$

Numerous experimental determinations of the constants A and B provide $A = 2.44$ and $B = 5.2$ within a 5% error (Pope, 2000). Tradition has it to write

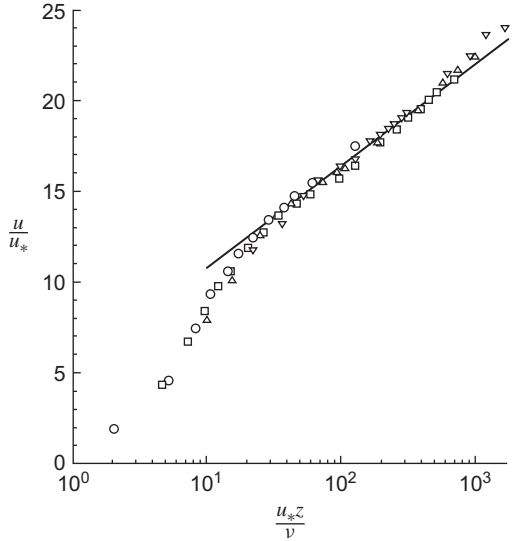

FIGURE 8.1 Mean velocity profiles in fully developed turbulent channel flow measured by Wei and Willmarth (1989) at various Reynolds numbers: circles $Re = 2970$, squares $Re = 14914$, upright triangles $Re = 22776$, and downright triangles $Re = 39582$. The straight line on this log-linear plot corresponds to the logarithmic profile of Eq. (8.2). (*From Pope, 2000*)

the function as:

$$u(z) = \frac{u_*}{\mathcal{K}} \ln \frac{u_* z}{\nu} + 5.2 u_*, \tag{8.4}$$

where $\mathcal{K} = 1/A = 0.41$ is called the *von Kármán constant*[1]

The portion of the curve closer to the wall, where the logarithmic law fails, may be approximated by the laminar solution. Constant laminar stress $\nu \mathrm{d}u/\mathrm{d}z = \tau_\mathrm{b}/\rho = u_*^2$ implies $u(z) = u_*^2 z/\nu$ there. Ignoring the region of transition in which the velocity profile gradually changes from one solution to the other, we can attempt to connect the two. Doing so yields $u_* z/\nu = 11$. This sets the thickness of the laminar boundary layer δ as the value of z for which $u_* z/\nu = 11$, that is,

$$\delta = 11 \frac{\nu}{u_*}. \tag{8.5}$$

Most textbooks (e.g., Kundu, 1990) give $\delta = 5\nu/u_*$, for the region in which the velocity profile is strictly laminar, and label the region between $5\nu/u_*$

[1] In honor of Theodore von Kármán (1881–1963), Hungarian-born physicist and engineer who made significant contributions to fluid mechanics while working in Germany and who first introduced this notation.

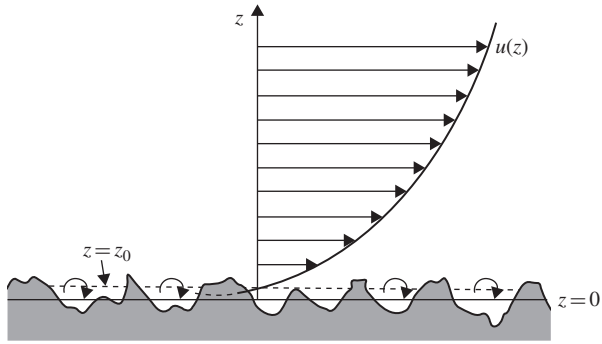

FIGURE 8.2 Velocity profile in the vicinity of a rough wall. The roughness height z_0 is smaller than the averaged height of the surface asperities. So, the velocity u falls to zero somewhere within the asperities, where local flow degenerates into small vortices between the peaks, and the negative values predicted by the logarithmic profile are not physically realized.

and $30\nu/u_*$ as the *buffer layer*, the transition zone between laminar and fully turbulent flow.

For water in ambient conditions, the molecular viscosity ν is equal to $1.0 \times 10^{-6}\,\mathrm{m^2/s}$, whereas the friction velocity in the ocean rarely falls below 1 mm/s. This implies that δ hardly exceeds a centimeter in the ocean and is almost always smaller than the height of the cobbles, ripples, and other asperities that typically line the bottom of the ocean basin. Similarly for the atmosphere, the air viscosity at ambient temperature and pressure is about $1.5 \times 10^{-5}\,\mathrm{m^2/s}$, and u_* rarely falls below 1 cm/s, giving $\delta < 5$ cm, smaller than most irregularities on land and wave heights at sea.

When this is the case, the velocity profile above the bottom asperities no longer depends on the molecular viscosity of the fluid but on the so-called *roughness height* z_0, such that

$$u(z) = \frac{u_*}{\mathcal{K}} \ln \frac{z}{z_0}, \tag{8.6}$$

as depicted in Fig. 8.2. It is important to note that the roughness height is not the average height of bumps on the surface but is a small fraction of it, about one tenth (Garratt, 1992, page 87).

8.1.2 Eddy Viscosity

We have already mentioned in Section 5.2 what an eddy diffusivity or viscosity is and how it can be formulated in the case of a homogeneous turbulence field, that is, away from boundaries. Near a boundary, the turbulence ceases to be isotropic and an alternate formulation needs to be developed.

In analogy with Newton's law for viscous fluids, which has the tangential stress τ proportional to the velocity shear $\mathrm{d}u/\mathrm{d}z$ with the coefficient of

proportionality being the molecular viscosity ν, we write for turbulent flow:

$$\tau = \rho_0 \nu_E \frac{du}{dz}, \tag{8.7}$$

where the turbulent viscosity ν_E supersedes the molecular viscosity ν. For the logarithmic profile (8.6) of a flow along a rough surface, the velocity shear is $du/dz = u_*/\mathcal{K}z$ and the stress τ is uniform across the flow (at least in the vicinity of the boundary for lack of other significant forces): $\tau = \tau_b = \rho u_*^2$, giving

$$\rho_0 u_*^2 = \rho_0 \nu_E \frac{u_*}{\mathcal{K}z}$$

and thus

$$\nu_E = \mathcal{K} z u_*. \tag{8.8}$$

Note that unlike the molecular viscosity, the turbulent viscosity is not constant in space, for it is not a property of the fluid but of the flow, including its structure. From its dimension (L^2T^{-1}), we verify that Eq. (8.8) is dimensionally correct and note that it can be expressed as the product of a length by the friction velocity:

$$\nu_E = l_m u_*, \tag{8.9}$$

with the *mixing length* l_m defined as

$$l_m = \mathcal{K} z. \tag{8.10}$$

This parameterization is occasionally used for cases other than boundary layers (see Chapter 14).

The preceding considerations ignored the effect of rotation. When rotation is present, the character of the boundary layer changes dramatically.

8.2 FRICTION AND ROTATION

After the development of the equations governing geophysical motions (Sections 4.1 to 4.4), a scale analysis was performed to evaluate the relative importance of the various terms (Section 4.5). In the horizontal momentum equations [(4.21a) and (4.21b)], each term was compared with the Coriolis term, and a corresponding dimensionless ratio was defined. For vertical friction, the dimensionless ratio was the *Ekman number*:

$$Ek = \frac{\nu_E}{\Omega H^2}, \tag{8.11}$$

where ν_E is the eddy viscosity, Ω the ambient rotation rate, and H the height (depth) scale of the motion (the total thickness if the fluid is homogeneous).

Typical geophysical flows, as well as laboratory experiments, are characterized by very small Ekman numbers. For example, in the ocean at midlatitudes ($\Omega \simeq 10^{-4}$ s^{-1}), motions modeled with an eddy-intensified viscosity $\nu_E = 10^{-2}$ m^2/s (much larger than the molecular viscosity of water, equal to 1.0×10^{-6} m^2/s) and extending over a depth of about 1000 m have an Ekman number of about 10^{-4}.

The smallness of the Ekman number indicates that vertical friction plays a very minor role in the balance of forces and may, consequently, be omitted from the equations. This is usually done and with great success. However, something is then lost. The frictional terms happen to be those with the highest order of derivatives among all terms of the momentum equations. Thus, when friction is neglected, the order of the set of differential equations is reduced, and not all boundary conditions can be applied simultaneously. Usually, slipping along the bottom must be accepted.

Since Ludwig Prandtl[2] and his general theory of boundary layers, we know that in such a circumstance, the fluid system exhibits two distinct behaviors: At some distance from the boundaries, in what is called the *interior*, friction is usually negligible, whereas, near a boundary (wall) and across a short distance, called the *boundary layer*, friction acts to bring the finite interior velocity to zero at the wall.

The thickness, d, of this thin layer is such that the Ekman number is on the order of one at that scale, allowing friction to be a dominant force:

$$\frac{\nu_E}{\Omega d^2} \sim 1,$$

which leads to

$$d \sim \sqrt{\frac{\nu_E}{\Omega}}. \tag{8.12}$$

Obviously, d is much less than H, and the boundary layer occupies a very small portion of the flow domain. For the oceanic values cited above ($\nu_E = 10^{-2}$ m^2/s and $\Omega = 10^{-4}$ s^{-1}), d is about 10 m.

Because of the Coriolis effect, the frictional boundary layer of geophysical flows, called the *Ekman layer*, differs greatly from the boundary layer in nonrotating fluids. Although, the traditional boundary layer has no particular thickness and grows either downstream or with time, the existence of the depth scale d in rotating fluids suggests that the Ekman layer can be characterized by a fixed thickness. (Note that as the rotational effects disappear ($\Omega \to 0$), d tends to infinity, exemplifying this essential difference between rotating and nonrotating fluids.) Rotation not only imparts a fixed length scale to the boundary layer, but we will now show that it also changes the direction of the velocity vector when approaching the boundary, leading to transverse currents.

[2] See biography at the end of this chapter.

8.3 THE BOTTOM EKMAN LAYER

Let us consider a uniform, geostrophic flow in a homogeneous fluid over a flat bottom (Fig. 8.3). This bottom exerts a frictional stress against the flow, bringing the velocity gradually to zero within a thin layer above the bottom. We now solve for the structure of this layer.

In the absence of horizontal gradients (the interior flow is said to be uniform) and of temporal variations, continuity equation (4.21d) yields $\partial w/\partial z = 0$ and thus $w = 0$ in the thin layer near the bottom. The remaining equations are the following reduced forms of Eq. (4.21a) through Eq. (4.21c):

$$-fv = -\frac{1}{\rho_0}\frac{\partial p}{\partial x} + \nu_E \frac{\partial^2 u}{\partial z^2} \tag{8.13a}$$

$$+fu = -\frac{1}{\rho_0}\frac{\partial p}{\partial y} + \nu_E \frac{\partial^2 v}{\partial z^2} \tag{8.13b}$$

$$0 = -\frac{1}{\rho_0}\frac{\partial p}{\partial z}, \tag{8.13c}$$

where f is the Coriolis parameter (taken as a constant here), ρ_0 is the fluid density, and ν_E is the eddy viscosity (taken as a constant for simplicity). The horizontal gradient of the pressure p is retained because a uniform flow requires a uniformly varying pressure (Section 7.1). For convenience, we align the x-axis with the direction of the interior flow, which is of velocity $\bar{u}$. The boundary conditions are then

$$\text{Bottom } (z = 0): \quad u = 0, \quad v = 0, \tag{8.14a}$$

$$\text{Toward the interior } (z \gg d): \quad u = \bar{u}, \quad v = 0, \quad p = \bar{p}(x, y). \tag{8.14b}$$

By virtue of Eq. (8.13c), the dynamic pressure p is the same at all depths; thus, $p = \bar{p}(x, y)$ in the interior flow as well as throughout the boundary layer.

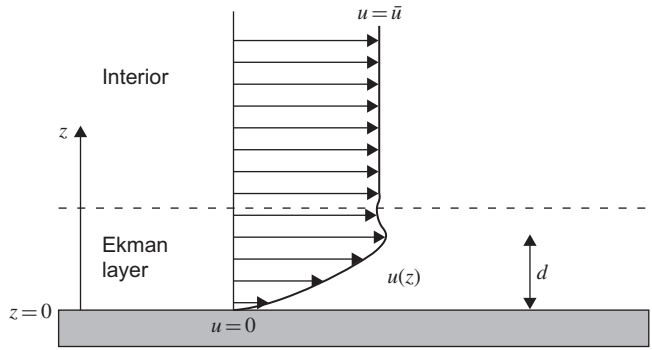

FIGURE 8.3 Frictional influence of a flat bottom on a uniform flow in a rotating framework.

In the interior flow ($z \gg d$, mathematically equivalent to $z \to \infty$), Eqs. (8.13a) and (8.13b) relate the velocity to the pressure gradient:

$$0 = -\frac{1}{\rho_0}\frac{\partial \bar{p}}{\partial x},$$
$$f\bar{u} = -\frac{1}{\rho_0}\frac{\partial \bar{p}}{\partial y} = \text{independent of } z.$$

Substitution of these derivatives in the same equations, which are now taken at any depth, yields

$$-fv = \nu_E \frac{d^2 u}{dz^2} \tag{8.15a}$$
$$f(u - \bar{u}) = \nu_E \frac{d^2 v}{dz^2}. \tag{8.15b}$$

Seeking a solution of the type $u = \bar{u} + A\exp(\lambda z)$ and $v = B\exp(\lambda z)$, we find that λ obeys $\nu^2\lambda^4 + f^2 = 0$; that is,

$$\lambda = \pm(1 \pm \mathrm{i})\frac{1}{d}$$

where the distance d is defined by

$$d = \sqrt{\frac{2\nu_E}{f}}. \tag{8.16}$$

Here, we have restricted ourselves to cases with positive f (northern hemisphere). Note the similarity to Eq. (8.12). Boundary conditions (8.14b) rule out the exponentially growing solutions, leaving

$$u = \bar{u} + e^{-z/d}\left(A\cos\frac{z}{d} + B\sin\frac{z}{d}\right) \tag{8.17a}$$
$$v = e^{-z/d}\left(B\cos\frac{z}{d} - A\sin\frac{z}{d}\right), \tag{8.17b}$$

and the application of the remaining boundary conditions (8.14a) yields $A = -\bar{u}$, $B = 0$, or

$$u = \bar{u}\left(1 - e^{-z/d}\cos\frac{z}{d}\right) \tag{8.18a}$$
$$v = \bar{u}e^{-z/d}\sin\frac{z}{d}. \tag{8.18b}$$

This solution has a number of important properties. First and foremost, we notice that the distance over which it approaches the interior solution is on the order of d. Thus, expression (8.16) gives the thickness of the boundary layer. For

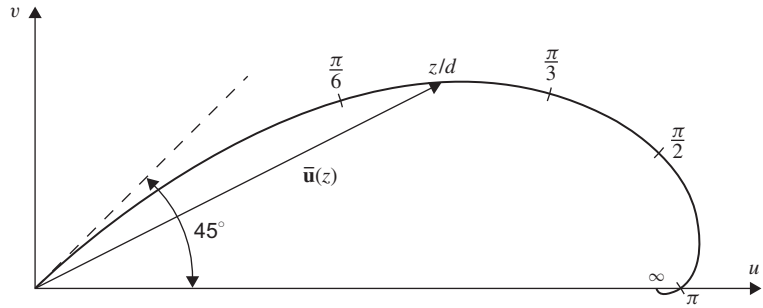

FIGURE 8.4 The velocity spiral in the bottom Ekman layer. The figure is drawn for the northern hemisphere ($f > 0$), and the deflection is to the left of the current above the layer. The reverse holds for the southern hemisphere.

this reason, d is called the *Ekman depth*. A comparison with Eq. (8.12) confirms the earlier argument that the boundary-layer thickness is the one corresponding to a local Ekman number near unity.

The preceding solution also tells us that there is, in the boundary layer, a flow transverse to the interior flow ($v \neq 0$). Very near the bottom ($z \to 0$), this component is equal to the downstream velocity ($u \sim v \sim \bar{u}z/d$), thus implying that the near-bottom velocity is at 45 degrees to the left of the interior velocity (Fig. 8.4). (The boundary flow is to the right of the interior flow for $f < 0$.) Further up, where u reaches a first maximum ($z = 3\pi d/4$), the velocity in the direction of the flow is greater than in the interior ($u = 1.07\bar{u}$). (Viscosity can occasionally fool us!)

It is instructive to calculate the net transport of fluid transverse to the main flow:

$$\mathrm{V} = \int_0^\infty v \, \mathrm{d}z = \frac{\bar{u}d}{2}, \tag{8.19}$$

which is proportional to the interior velocity and the Ekman depth.

8.4 GENERALIZATION TO NONUNIFORM CURRENTS

Let us now consider a more complex interior flow, namely, a spatially nonuniform flow that is varying on a scale sufficiently large to be in geostrophic equilibrium (low Rossby number, as in Section 7.1). Thus,

$$-f\bar{v} = -\frac{1}{\rho_0}\frac{\partial \bar{p}}{\partial x}, \quad f\bar{u} = -\frac{1}{\rho_0}\frac{\partial \bar{p}}{\partial y},$$

where the pressure $\bar{p}(x, y, t)$ is arbitrary. For a constant Coriolis parameter, this flow is nondivergent ($\partial\bar{u}/\partial x + \partial\bar{v}/\partial y = 0$). The boundary-layer equations are now

$$-f(v-\bar{v}) = \nu_E \frac{\partial^2 u}{\partial z^2} \tag{8.20a}$$

$$f(u-\bar{u}) = \nu_E \frac{\partial^2 v}{\partial z^2}, \tag{8.20b}$$

and the solution that satisfies the boundary conditions aloft ($u \to \bar{u}$ and $v \to \bar{v}$ for $z \to \infty$) is

$$u = \bar{u} + e^{-z/d}\left(A\cos\frac{z}{d} + B\sin\frac{z}{d}\right) \tag{8.21}$$

$$v = \bar{v} + e^{-z/d}\left(B\cos\frac{z}{d} - A\sin\frac{z}{d}\right). \tag{8.22}$$

Here, the "constants" of integration A and B are independent of z but will be dependent on x and y through $\bar{u}$ and $\bar{v}$. Imposing $u = v = 0$ along the bottom ($z = 0$) sets their values, and the solution is

$$u = \bar{u}\left(1 - e^{-z/d}\cos\frac{z}{d}\right) - \bar{v}e^{-z/d}\sin\frac{z}{d} \tag{8.23a}$$

$$v = \bar{u}e^{-z/d}\sin\frac{z}{d} + \bar{v}\left(1 - e^{-z/d}\cos\frac{z}{d}\right). \tag{8.23b}$$

The transport attributed to the boundary-layer flow has components given by

$$\mathrm{U} = \int_0^\infty (u-\bar{u})\,\mathrm{d}z = -\frac{d}{2}(\bar{u}+\bar{v}) \tag{8.24a}$$

$$\mathrm{V} = \int_0^\infty (v-\bar{v})\,\mathrm{d}z = \frac{d}{2}(\bar{u}-\bar{v}). \tag{8.24b}$$

Since this transport is not necessarily parallel to the interior flow, it is likely to have a nonzero divergence. Indeed,

$$\frac{\partial \mathrm{U}}{\partial x} + \frac{\partial \mathrm{V}}{\partial y} = \int_0^\infty \left(\frac{\partial u}{\partial x} + \frac{\partial v}{\partial y}\right)\mathrm{d}z = -\frac{d}{2}\left(\frac{\partial \bar{v}}{\partial x} - \frac{\partial \bar{u}}{\partial y}\right)$$

$$= -\frac{d}{2\rho_0 f}\nabla^2\bar{p}. \tag{8.25}$$

The flow in the boundary layer converges or diverges if the interior flow has a relative vorticity. The situation is depicted in Fig. 8.5. The question is: From where does the fluid come, or where does it go, to meet this convergence

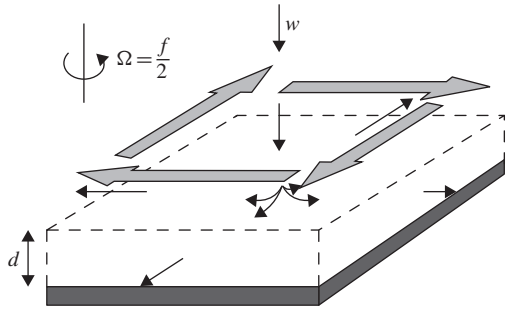

FIGURE 8.5 Divergence in the bottom Ekman layer and compensating downwelling in the interior. Such a situation arises in the presence of an anticyclonic gyre in the interior, as depicted by the large horizontal arrows. Similarly, interior cyclonic motion causes convergence in the Ekman layer and upwelling in the interior.

or divergence? Because of the presence of a solid bottom, the only possibility is that it be supplied from the interior by means of a vertical velocity. But, remember (Section 7.1) that geostrophic flows must be characterized by

$$\frac{\partial \bar{w}}{\partial z} = 0, \tag{8.26}$$

that is, the vertical velocity must occur throughout the depth of the fluid. Of course, since the divergence of the flow in the Ekman layer is proportional to the Ekman depth, d, which is very small, this vertical velocity is weak.

The vertical velocity in the interior, called *Ekman pumping*, can be evaluated by a vertical integration of the continuity equation (4.21d), using $w(z=0)=0$ and $w(z\to\infty)=\bar{w}$:

$$\begin{aligned}\bar{w} &= -\int_0^\infty \left(\frac{\partial u}{\partial x}+\frac{\partial v}{\partial y}\right) dz = \frac{d}{2}\left(\frac{\partial \bar{v}}{\partial x}-\frac{\partial \bar{u}}{\partial y}\right) \\ &= \frac{d}{2\rho_0 f}\nabla^2\bar{p} = \frac{1}{\rho_0}\sqrt{\frac{\nu_E}{2f^3}}\nabla^2\bar{p}.\end{aligned} \tag{8.27}$$

So, the greater the vorticity of the mean flow, the greater the upwelling or downwelling. Also, the effect increases toward the equator (decreasing $f = 2\Omega\sin\varphi$ and increasing d). The direction of the vertical velocity is upward in a cyclonic flow (counterclockwise in the northern hemisphere) and downward in an anticyclonic flow (clockwise in the northern hemisphere).

In the southern hemisphere, where $f<0$, the Ekman layer thickness d must be redefined with the absolute value of f: $d=\sqrt{2\nu_E/|f|}$, but the previous rule remains: the vertical velocity is upward in a cyclonic flow and downward in an anticyclonic flow. The difference is that cyclonic flow is clockwise and anticyclonic flow is counterclockwise.

8.5 THE EKMAN LAYER OVER UNEVEN TERRAIN

It is noteworthy to explore how an irregular topography may affect the structure of the Ekman layer and, in particular, the magnitude of the vertical velocity in the interior. For this, consider a horizontal geostrophic interior flow $(\bar{u}, \bar{v})$, not necessarily spatially uniform, over an uneven terrain of elevation $z=b(x,y)$ above a horizontal reference level. To be faithful to our restriction (Section 4.3) to geophysical flows much wider than they are thick, we shall assume that the bottom slope $(\partial b/\partial x,\ \partial b/\partial y)$ is everywhere small ($\ll 1$). This is hardly a restriction in most atmospheric and oceanic situations.

Our governing equations are again (8.20), coupled to the continuity equation (4.21d), but the boundary conditions are now

$$\text{Bottom } (z=b): \quad u=0,\ \ v=0,\ \ w=0, \tag{8.28}$$

$$\text{Toward the interior } (z\gg b+d): \quad u=\bar{u},\ \ v=\bar{v}. \tag{8.29}$$

The solution is the previous solution (8.23) with z replaced by $z-b$:

$$u=\bar{u}-\mathrm{e}^{(b-z)/d}\left(\bar{u}\cos\frac{z-b}{d}+\bar{v}\sin\frac{z-b}{d}\right) \tag{8.30a}$$

$$v=\bar{v}+\mathrm{e}^{(b-z)/d}\left(\bar{u}\sin\frac{z-b}{d}-\bar{v}\cos\frac{z-b}{d}\right). \tag{8.30b}$$

We note that the vertical thickness of the boundary layer is still measured by $d=\sqrt{2\nu_{\mathrm{E}}/f}$. However, the boundary layer is now oblique, and its true thickness, measured perpendicularly to the bottom, is slightly reduced by the cosine of the small bottom slope.

The vertical velocity is then determined from the continuity equation:

$$\begin{aligned}\frac{\partial w}{\partial z}&=-\frac{\partial u}{\partial x}-\frac{\partial v}{\partial y}\\&=\mathrm{e}^{(b-z)/d}\left\{\left(\frac{\partial\bar{v}}{\partial x}-\frac{\partial\bar{u}}{\partial y}\right)\sin\frac{z-b}{d}\right.\\&\quad+\frac{1}{d}\frac{\partial b}{\partial x}\left[(\bar{u}-\bar{v})\cos\frac{z-b}{d}+(\bar{u}+\bar{v})\sin\frac{z-b}{d}\right]\\&\quad\left.+\frac{1}{d}\frac{\partial b}{\partial y}\left[(\bar{u}+\bar{v})\cos\frac{z-b}{d}-(\bar{u}-\bar{v})\sin\frac{z-b}{d}\right]\right\},\end{aligned}$$

where use has been made of the fact that the interior geostrophic flow has no divergence [$\partial\bar{u}/\partial x+\partial\bar{v}/\partial y=0$ – See (7.5)]. A vertical integration from the bottom ($z=b$), where the vertical velocity vanishes ($w=0$ because u and v are also zero there) into the interior ($z\to+\infty$) where the vertical velocity assumes a vertically uniform value ($w=\bar{w}$), yields

$$\bar{w}=\left(\bar{u}\frac{\partial b}{\partial x}+\bar{v}\frac{\partial b}{\partial y}\right)+\frac{d}{2}\left(\frac{\partial\bar{v}}{\partial x}-\frac{\partial\bar{u}}{\partial y}\right). \tag{8.31}$$

The interior vertical velocity thus consists of two parts: a component that ensures no normal flow to the bottom [see (7.7)] and an Ekman-pumping contribution, as if the bottom were horizontally flat [see (8.27)].

The vanishing of the flow component perpendicular to the bottom must be met by the inviscid dynamics of the interior, giving rise to the first contribution to $\bar{w}$. The role of the boundary layer is to bring the tangential velocity to zero at the bottom. This explains the second contribution to $\bar{w}$. Note that the Ekman pumping is not affected by the bottom slope.

The preceding solution can also be applied to the lower portion of the atmospheric boundary layer. This was first done by Akerblom (1908), and matching between the logarithmic layer close to the ground (Section 8.1.1) and the Ekman layer further aloft was performed by Van Dyke (1975). Oftentimes, however, the lower atmosphere is in a stable (stratified) or unstable (convecting) state, and the neutral state during which Ekman dynamics prevail is more the exception than the rule.

8.6 THE SURFACE EKMAN LAYER

An Ekman layer occurs not only along bottom surfaces, but wherever there is a horizontal frictional stress. This is the case, for example, along the ocean surface, where waters are subject to a wind stress. In fact, this is precisely the situation first examined by Vagn Walfrid Ekman.[3] Fridtjof Nansen[4] had noticed during his cruises to northern latitudes that icebergs drift not downwind but systematically at some angle to the right of the wind. Ekman, his student at the time, reasoned that the cause of this bias was the earth's rotation and subsequently developed the mathematical representation that now bears his name. The solution was originally published in his 1902 doctoral thesis and again, in a more complete article, three years later (Ekman, 1905). In a subsequent article (Ekman, 1906), he mentioned the relevance of his theory to the lower atmosphere, where the wind approaches a geostrophic value with increasing height.

Let us consider the situation depicted in Fig. 8.6, where an ocean region with interior flow field $(\bar{u}, \bar{v})$ is subjected to a wind stress (τ^x, τ^y) along its surface. Again, assuming steady conditions, a homogeneous fluid, and a geostrophic interior, we obtain the following equations and boundary conditions for the flow field (u, v) in the surface Ekman layer:

$$-f(v-\bar{v}) = \nu_E \frac{\partial^2 u}{\partial z^2} \tag{8.32a}$$

$$+f(u-\bar{u}) = \nu_E \frac{\partial^2 v}{\partial z^2} \tag{8.32b}$$

[3] See biography at the end of this chapter.

[4] Fridtjof Nansen (1861–1930), Norwegian oceanographer famous for his Arctic expeditions and Nobel Peace Prize laureate (1922).

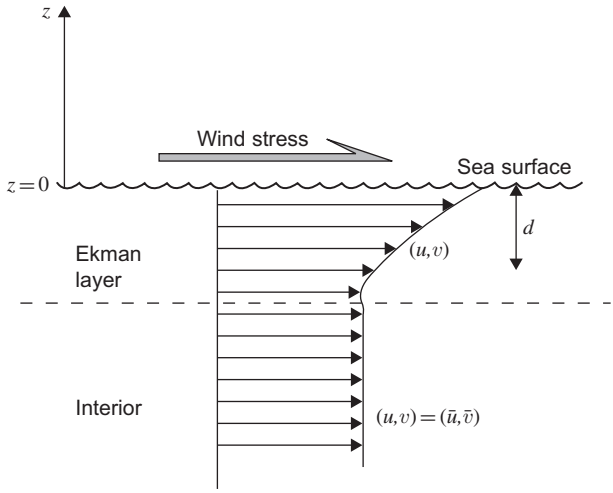

FIGURE 8.6 The surface Ekman layer generated by a wind stress on the ocean.

$$\text{Surface } (z=0): \quad \rho_0 \nu_E \frac{\partial u}{\partial z} = \tau^x, \quad \rho_0 \nu_E \frac{\partial v}{\partial z} = \tau^y \tag{8.32c}$$

$$\text{Toward interior } (z \to -\infty): \quad u = \bar{u}, \quad v = \bar{v}. \tag{8.32d}$$

The solution to this problem is

$$u = \bar{u} + \frac{\sqrt{2}}{\rho_0 f d} e^{z/d} \left[\tau^x \cos\left(\frac{z}{d} - \frac{\pi}{4}\right) - \tau^y \sin\left(\frac{z}{d} - \frac{\pi}{4}\right) \right] \tag{8.33a}$$

$$v = \bar{v} + \frac{\sqrt{2}}{\rho_0 f d} e^{z/d} \left[\tau^x \sin\left(\frac{z}{d} - \frac{\pi}{4}\right) + \tau^y \cos\left(\frac{z}{d} - \frac{\pi}{4}\right) \right], \tag{8.33b}$$

in which we note that the departure from the interior flow ($\bar{u}$, $\bar{v}$) is exclusively due to the wind stress. In other words, it does not depend on the interior flow. Moreover, this wind-driven flow component is inversely proportional to the Ekman-layer depth, d, and may be very large. Physically, if the fluid is almost inviscid (small ν_E, hence short d), a moderate surface stress can generate large drift velocities.

The wind-driven horizontal transport in the surface Ekman layer has components given by

$$U = \int_{-\infty}^{0} (u - \bar{u})\, dz = \frac{1}{\rho_0 f} \tau^y \tag{8.34a}$$

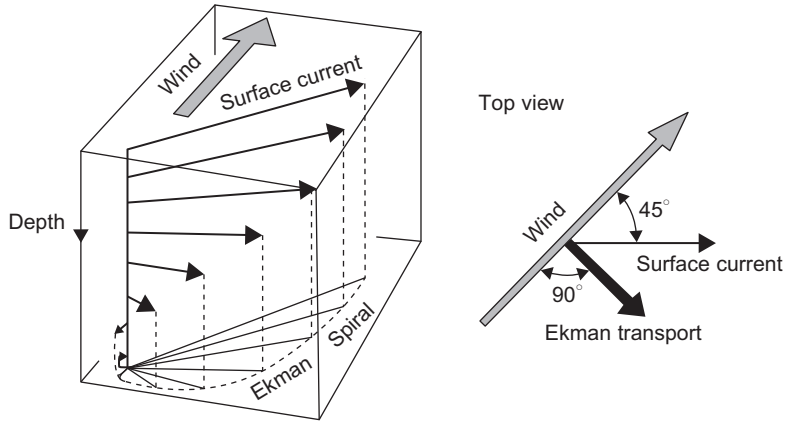

FIGURE 8.7 Structure of the surface Ekman layer. The figure is drawn for the northern hemisphere ($f > 0$), and the deflection is to the right of the surface stress. The reverse holds for the southern hemisphere.

$$\mathrm{V} = \int_{-\infty}^{0} (v - \bar{v})\, \mathrm{d}z = \frac{-1}{\rho_0 f} \tau^x. \tag{8.34b}$$

Surprisingly, it is oriented perpendicular to the wind stress (Fig. 8.7), to the right in the northern hemisphere and to the left in the southern hemisphere. This fact explains why icebergs, which float mostly underwater, systematically drift to the right of the wind in the North Atlantic, as observed by Fridtjof Nansen.

As for the bottom Ekman layer, let us determine the divergence of the flow, integrated over the boundary layer:

$$\int_{-\infty}^{0} \left(\frac{\partial u}{\partial x} + \frac{\partial v}{\partial y} \right) \mathrm{d}z = \frac{1}{\rho_0} \left[\frac{\partial}{\partial x} \left(\frac{\tau^y}{f} \right) - \frac{\partial}{\partial y} \left(\frac{\tau^x}{f} \right) \right]. \tag{8.35}$$

At constant f, the contribution is entirely due to the wind stress since the interior geostrophic flow is nondivergent. It is proportional to the wind-stress curl and, most importantly, it is independent of the value of the viscosity. It can be shown furthermore that this property continues to hold even when the turbulent eddy viscosity varies spatially (see Analytical Problem 8.7).

If the wind stress has a nonzero curl, the divergence of the Ekman transport must be provided by a vertical velocity throughout the interior. A vertical integration of the continuity equation, (4.21d), across the Ekman layer with $w(z = 0)$

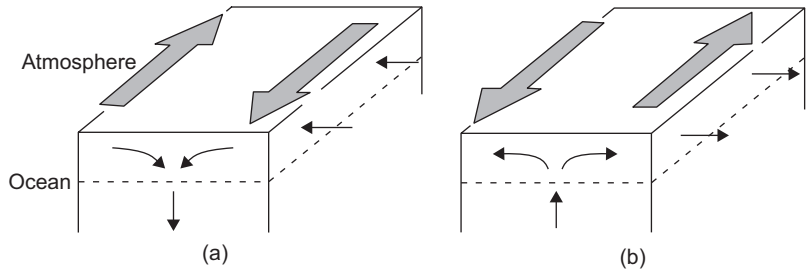

FIGURE 8.8 Ekman pumping in an ocean subject to sheared winds (case of northern hemisphere).

and $w(z \to -\infty) = \bar{w}$ yields

$$\begin{aligned} \bar{w} &= + \int_{-\infty}^{0} \left(\frac{\partial u}{\partial x} + \frac{\partial v}{\partial y} \right) \mathrm{d}z \\ &= \frac{1}{\rho_0} \left[\frac{\partial}{\partial x} \left(\frac{\tau^y}{f} \right) - \frac{\partial}{\partial y} \left(\frac{\tau^x}{f} \right) \right] = w_{\mathrm{Ek}}. \end{aligned} \tag{8.36}$$

This vertical velocity is called *Ekman pumping*. In the northern hemisphere ($f > 0$), a clockwise wind pattern (negative curl) generates a downwelling (Fig. 8.8a), whereas a counterclockwise wind pattern causes upwelling (Fig. 8.8b). The directions are opposite in the southern hemisphere. Ekman pumping is a very effective mechanism by which winds drive subsurface ocean currents (Pedlosky, 1996; see also Chapter 20).

8.7 THE EKMAN LAYER IN REAL GEOPHYSICAL FLOWS

The preceding models of bottom and surface Ekman layers are highly idealized, and we do not expect their solutions to match actual atmospheric and oceanic observations closely (except in some cases; see Fig. 8.9). Three factors, among others, account for substantial differences: turbulence, stratification, and horizontal gradients.

It was noted at the end of Chapter 4 that geophysical flows have large Reynolds numbers and are therefore in a state of turbulence. Replacing the molecular viscosity of the fluid by a much greater eddy viscosity, as performed in Section 4.2, is a first attempt to recognize the enhanced transfer of momentum in a turbulent flow. However, in a shear flow such as in an Ekman layer, the turbulence is not homogeneous, being more vigorous where the shear is greater and also partially suppressed in the proximity of the boundary where the size of turbulent eddies is restricted. In the absence of an exact theory of

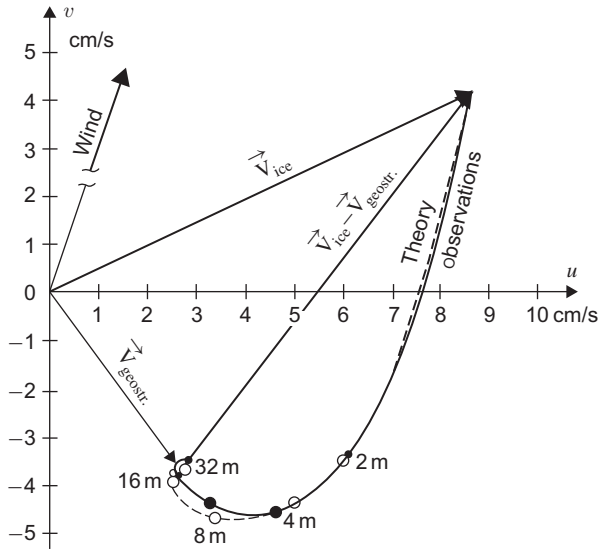

FIGURE 8.9 Comparison between observed currents below a drifting ice floe at 84.3°N and theoretical predictions based on an eddy viscosity $\nu_E = 2.4 \times 10^{-3}$ m^2/s. (*Reprinted from Deep-Sea Research, 13, Kenneth Hunkins, Ekman drift currents in the Arctic Ocean, p. 614, ©1966, with kind permission from Pergamon Press Ltd, Headington Hill Hall, Oxford 0X3 0BW, UK*)

turbulence, several schemes have been proposed. For the bottom layer, the eddy viscosity has been made to vary in the vertical (Madsen, 1977) and to depend on the bottom stress (Cushman-Roisin & Malačič, 1997). Other schemes have been formulated (see Section 4.2), with varying degrees of success. Despite numerous disagreements among models and with field observations, two results nonetheless stand out as quite general. The first is that the angle between the near-boundary velocity and that in the interior or that of the surface stress (depending on the type of Ekman layer) is always substantially less than the theoretical value of 45° and is found to range between 5° and 20° (Fig. 8.10). See also Stacey, Pond and LeBlond (1986).

The second result is a formula for the vertical scale of the Ekman-layer thickness:

$$d \simeq 0.4 \, \frac{u_*}{f}, \tag{8.37}$$

where u_* is the turbulent friction velocity defined in Eq. (8.1). The numerical factor is derived from observations (Garratt, 1992, Appendix 3). Although 0.4 is the most commonly accepted value, there is evidence that certain oceanic conditions call for a somewhat smaller value (Mofjeld & Lavelle, 1984; Stigebrandt, 1985).

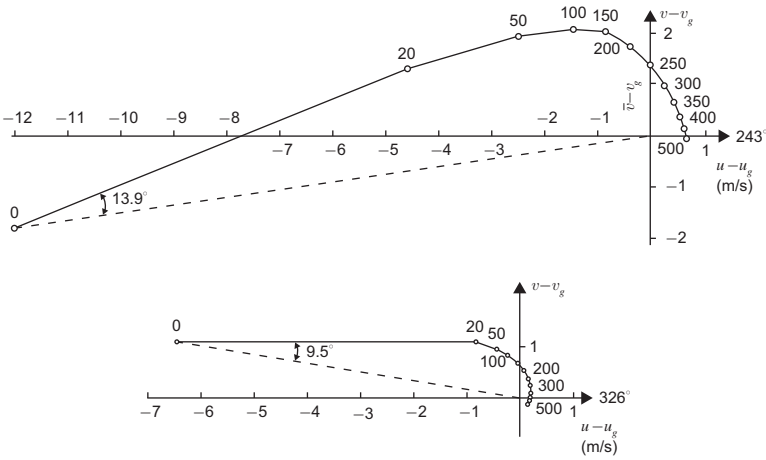

FIGURE 8.10 Wind vectors minus geostrophic wind as a function of height (in meters) in the maritime friction layer near the Scilly Isles. Top diagram: Case of warm air over cold water. Bottom diagram: Case of cold air over warm water. (*Adapted from Roll, 1965*)

Taking u_* as the turbulent velocity and the (unknown) Ekman-layer depth scale, d, as the size of the largest turbulent eddies, we write

$$\nu_E \sim u_* d. \tag{8.38}$$

Then, using rule (8.12) to determine the boundary-layer thickness, we obtain

$$1 \sim \frac{\nu_E}{fd^2} \sim \frac{u_*}{fd},$$

which immediately leads to Eq. (8.37).

The other major element missing from the Ekman-layer formulations of the previous sections is the presence of vertical density stratification. Although the effects of stratification are not discussed in detail until Chapter 11, it can be anticipated here that the gradual change of density with height (lighter fluid above heavier fluid) hinders vertical movements, thereby reducing vertical mixing of momentum by turbulence; it also allows the motions at separate levels to act less coherently and to generate internal gravity waves. As a consequence, stratification reduces the thickness of the Ekman layer and increases the veering of the velocity vector with height (Garratt, 1992, Section 6.2). For a study of the oceanic wind-driven Ekman layer in the presence of density stratification, the reader is referred to Price and Sundermeyer (1999).

The surface atmospheric layer during daytime over land and above warm currents at sea is frequently in a state of convection because of heating from below. In such situations, the Ekman dynamics give way to convective motions, and a controlling factor, besides the geostrophic wind aloft, is the intensity of the surface heat flux. An elementary model is presented later (Section 14.7).

Because Ekman dynamics then play a secondary role, the layer is simply called the *atmospheric boundary layer*. The interested reader is referred to books on the subject by Stull (1988), Sorbjan (1989), Zilitinkevich (1991), or Garratt (1992).

8.8 NUMERICAL SIMULATION OF SHALLOW FLOWS

The theory presented till now largely relies on the assumption of a constant turbulent viscosity. For real flows, however, turbulence is rarely uniform, and eddy diffusion profiles must be considered. Such complexity renders the analytical treatment tedious or even impossible, and numerical methods need to be employed.

To illustrate the approach, we reinstate nonstationary terms and assume a vertically varying eddy viscosity (Fig. 8.11) but retain the hydrostatic approximation (8.13c) and continue to consider a fluid of homogeneous density. The governing equations for u and v are

$$\frac{\partial u}{\partial t} - fv = -\frac{1}{\rho_0}\frac{\partial p}{\partial x} + \frac{\partial}{\partial z}\left(\nu_E(z)\frac{\partial u}{\partial z}\right) \tag{8.39a}$$

$$\frac{\partial v}{\partial t} + fu = -\frac{1}{\rho_0}\frac{\partial p}{\partial y} + \frac{\partial}{\partial z}\left(\nu_E(z)\frac{\partial v}{\partial z}\right) \tag{8.39b}$$

$$0 = -\frac{1}{\rho_0}\frac{\partial p}{\partial z}. \tag{8.39c}$$

From the last equation, it is clear that the horizontal pressure gradient is independent of z.

A standard finite-volume approach could be applied to the equations, but since we already used the approach several times, its implementation is left here as an exercise (see Numerical Problem 8.5). Instead, we introduce another

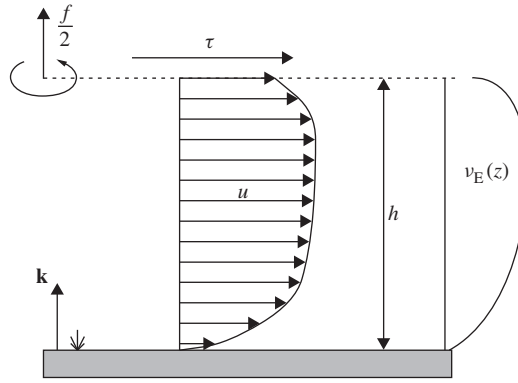

FIGURE 8.11 A vertically confined fluid flow, with bottom and top Ekman layers bracketing a nonuniform velocity profile. The vertical structure can be calculated by a one-dimensional model spanning the entire fluid column eventhough the turbulent viscosity $\nu_E(z)$ may vary in the vertical.

numerical method, which consists in expanding the solution in terms of preselected functions ϕ_j, called *basis functions*. A finite set of N basis functions is used to construct a *trial solution*:

$$\begin{aligned}\tilde{u}(z,t) &= a_1(t)\phi_1(z) + a_2(t)\phi_2(z) + \cdots + a_N(t)\phi_N(z) \\ &= \sum_{j=1}^{N} a_j(t)\,\phi_j(z) \qquad (8.40a)\\ \tilde{v}(z,t) &= b_1(t)\phi_1(z) + b_2(t)\phi_2(z) + \cdots + b_N(t)\phi_N(z) \\ &= \sum_{j=1}^{N} b_j(t)\,\phi_j(z). \qquad (8.40b)\end{aligned}$$

The problem then reduces to finding a way to calculate the unknown coefficients $a_j(t)$ and $b_j(t)$ for $j = 1$ to N such that the trial solution is as close as possible to the exact solution. In other words, we demand that the residual r_u obtained by substituting the trial solution $\tilde{u}$ into the differential x-momentum equation,

$$\frac{\partial \tilde{u}}{\partial t} - f\tilde{v} + \frac{1}{\rho_0}\frac{\partial p}{\partial x} - \frac{\partial}{\partial z}\left(\nu_E \frac{\partial \tilde{u}}{\partial z}\right) = r_u, \qquad (8.41)$$

be as small as possible, and similarly with the residual r_v of the y-momentum equation. The residuals r_u and r_v quantify the truncation error of the trial solution, and the objective is to minimize them.

Collocation methods require that the residuals be zero at a finite number of locations z_k across the domain. If each of the two series contains N terms, then taking also N points where the two residuals r_u and r_v are forced to vanish provides $2N$ constraints for the $2N$ unknowns a_j and b_j. With a little chance, these constraints will be necessary and sufficient to determine the time evolution of the coefficients $a_j(t)$ and $b_j(t)$. In the present case, the situation is almost certain because the equations are linear, and the temporal derivatives $\mathrm{d}a_j(t)/\mathrm{d}t$ and $\mathrm{d}b_j(t)/\mathrm{d}t$ appear in linear differential equations, a relatively straightforward problem to be solved numerically, though the matrices involved may have few zeros. In some cases, however, the equations may be ill-conditioned because of inadequate choices of the collocation points z_k (e.g., Gottlieb & Orszag, 1977).

An alternative to requiring zero residuals at selected points is to minimize a global measure of the error. For example, we can multiply the equations by N different weighting functions $\mathrm{w}_i(z)$ and integrate over the domain before requiring that the weighted-average error vanish:

$$\int_0^h \mathrm{w}_i r_u \,\mathrm{d}z = 0, \qquad (8.42)$$

and similarly for the companion equation. Note that we require Eq. (8.42) to hold only for a *finite set* of functions w_i, $i=1,\ldots,N$. Had we asked instead that the integral be zero for *any* function w, the trial solution would be the exact solution of the equation since r_u and r_v would then be zero everywhere, but this not possible because we have only $2N$ and not an infinity of degrees of freedom at our disposal. The weighted residuals (8.42) must satisfy

$$\int_0^h \mathrm{w}_i \left[\frac{\partial \tilde{u}}{\partial t} - f\tilde{v} + \frac{1}{\rho_0}\frac{\partial p}{\partial x} - \frac{\partial}{\partial z}\left(\nu_\mathrm{E}\frac{\partial \tilde{u}}{\partial z}\right)\right] \mathrm{d}z = 0, \tag{8.43}$$

for every value of the index i, which leads to

$$\sum_{j=1}^{N}\int_0^h \left(\mathrm{w}_i\phi_j\,\mathrm{d}z\right)\frac{\mathrm{d}a_j}{\mathrm{d}t} - f\sum_{j=1}^{N}\int_0^h \left(\mathrm{w}_i\phi_j\,\mathrm{d}z\right) b_j + \frac{1}{\rho_0}\frac{\partial p}{\partial x}\int_0^h (\mathrm{w}_i\,\mathrm{d}z)$$

$$-\mathrm{w}_i(h)\,\nu_\mathrm{E}\frac{\partial u}{\partial z}\bigg|_h + \mathrm{w}_i(0)\;\nu_\mathrm{E}\frac{\partial u}{\partial z}\bigg|_0 + \sum_{j=1}^{N}\int_0^h \left(\nu_\mathrm{E}\frac{\mathrm{d}\mathrm{w}_i}{\mathrm{d}z}\frac{\mathrm{d}\phi_j}{\mathrm{d}z}\,\mathrm{d}z\right) a_j = 0, \tag{8.44}$$

and similarly for the y-momentum equation, with the as replaced by bs, bs by $-a$s, x by y, and u by v. Note that use was made of the fact that the pressure gradient is independent of z. The top and bottom stresses (first and second terms of the last line) can be replaced by their value, if known (such as a wind stress on the sea surface).

As already mentioned, if Eq. (8.44) holds for any weighting function, an exact solution is obtained, but if it only holds for a finite series of weighting functions, an approximate solution is found for which the residual is not zero everywhere but is orthogonal to every weighting function.[5] If N different weights are used and the weighted residuals of each of the 2 equations are required to be zero, we obtain $2N$ ordinary differential equations for the $2N$ unknowns a_j and b_j. To write the sets of equations in compact form, we define square matrices $\mathbf{M}$ and $\mathbf{K}$ and column vector $\mathbf{s}$ by

$$M_{ij} = \int_0^h \mathrm{w}_i\phi_j\,\mathrm{d}z, \quad K_{ij} = \int_0^h \nu_\mathrm{E}\frac{\mathrm{d}\mathrm{w}_i}{\mathrm{d}z}\frac{\mathrm{d}\phi_j}{\mathrm{d}z}\,\mathrm{d}z, \quad s_i = \int_0^h \mathrm{w}_i\,\mathrm{d}z. \tag{8.45}$$

We then group the coefficients a_j and b_j into column vectors $\mathbf{a}$ and $\mathbf{b}$ and the functions $\mathrm{w}_i(z)$ into a column vector $\mathbf{w}(z)$. The weighted-residual equations can

[5] Orthogonality of two functions is understood here as the property that the product of the two functions integrated over the domain is zero. In the present case, the residual is orthogonal to all weighting functions.

then be written in matrix notation as

$$\mathbf{M}\frac{\mathrm{d}\mathbf{a}}{\mathrm{d}t} = +f\mathbf{M}\mathbf{b} - \mathbf{K}\mathbf{a} - \frac{1}{\rho_0}\frac{\partial p}{\partial x}\mathbf{s} + \frac{\tau^x}{\rho_0}\mathbf{w}(h) - \frac{\tau_\mathrm{b}^x}{\rho_0}\mathbf{w}(0) \tag{8.46a}$$

$$\mathbf{M}\frac{\mathrm{d}\mathbf{b}}{\mathrm{d}t} = -f\mathbf{M}\mathbf{a} - \mathbf{K}\mathbf{b} - \frac{1}{\rho_0}\frac{\partial p}{\partial y}\mathbf{s} + \frac{\tau^y}{\rho_0}\mathbf{w}(h) - \frac{\tau_\mathrm{b}^y}{\rho_0}\mathbf{w}(0). \tag{8.46b}$$

This set of ordinary differential equations can be solved by any of the time-integration methods of Chapter 2 as long as the temporal evolution of the surface stress, bottom stress, and pressure gradient is known.

There remains to provide an initial condition on the coefficients a_j and b_j, which must be deduced from the initial flow condition (see Numerical Exercise 8.1). After solving Eq. (8.46), the known values of the coefficients $a_j(t)$ and $b_j(t)$ permit the reconstruction of the solution by means of expansion (8.40). This method is called the *weighted-residual method*.

A word of caution is necessary with respect to boundary conditions. Top and bottom conditions on the shear stress are automatically taken into account, since the stress appears explicitly in the discrete formulation. A Neumann boundary condition, called a *natural condition*, is thus easily applied. No special demand is placed on the basis functions, and weights are simply required to be different from zero at boundaries where a stress condition is applied. There are situations, however, when the stress on the boundary is not known. This is generally the case at a solid boundary along which a no-slip boundary condition $u = v = 0$ is enforced. The integration method does not make the boundary values of u and v appear, and the basis functions must be chosen carefully to be compatible with the boundary condition. In the case of a no-slip condition, it is required that $\phi_j = 0$ at the concerned boundary, so that the velocity is made to vanish there. This is called an *essential boundary condition*.

Till now, both basis functions ϕ_j and weights w_i were arbitrary, except for the aforementioned boundary-related constraints, and smart choices can lead to effective methods. The *Galerkin method* makes the rather natural choice of taking weights equal to the basis functions used in the expansion. The error is then orthogonal to the basis functions. With a well-chosen set of functions ϕ_j, an increasing number of functions can be made to lead ultimately to the exact solution. With the Galerkin method, the matrices $\mathbf{M}$ and $\mathbf{K}$ are symmetric, with components[6]:

$$M_{ij} = \int_0^h \phi_i\phi_j\,\mathrm{d}z, \quad K_{ij} = \int_0^h \nu_\mathrm{E}\frac{\mathrm{d}\phi_i}{\mathrm{d}z}\frac{\mathrm{d}\phi_j}{\mathrm{d}z}\,\mathrm{d}z, \quad s_i = \int_0^h \phi_i\,\mathrm{d}z. \tag{8.47}$$

The basis functions ϕ_j do not need to span the entire domain but may be chosen to be zero everywhere, except in finite subdomains. The solution can

[6] In finite-element jargon, $\mathbf{M}$ and $\mathbf{K}$ are called, respectively, the mass matrix and stiffness matrix.

then be interpreted as the superposition of elementary local solutions. For this, the numerical domain is divided into subdomains called *finite elements*, which are linear segments in 1D, triangles in 2D, and on each of which only a few basis functions differ from zero. This greatly reduces the calculations of the matrices $\mathbf{M}$ and $\mathbf{K}$. The finite-element method is one of the most advanced and flexible methods available for the solution of partial differential equations but is also one of the most difficult to implement correctly (see, e.g., Hanert, Legat & Deleersnijder, 2003 for the implementation of a 2D ocean model). The interested reader is referred to the specialized literature: Buchanan (1995) and Zienkiewicz and Taylor (2000) for an introduction to general finite-element methods, and Zienkiewicz, Taylor and Nithiarasu (2005) for the application of finite elements to fluid dynamics.

For the bottom boundary condition $u = v = 0$, one takes $w_j(0) = \phi_j(0) = 0$, and Eq. (8.46) are unchanged, except for the fact that the term including the bottom stress disappears. The method involves matrices coupling all unknowns a_j and b_j, demanding a preliminary matrix inversion (N^3 operations) and then matrix-vector multiplications (N^2 operations) at every time step.

For the 1D Ekman layer, the problem can be further simplified (e.g., Davies, 1987; Heaps, 1987) by choosing special basis functions that are designed to obey

$$\frac{\partial}{\partial z}\left(\nu_{\mathrm{E}}(z)\,\frac{\partial \phi_j}{\partial z}\right) = -\varrho_j\,\phi_j(z) \tag{8.48a}$$

$$\phi_i(0) = 0, \qquad \left.\frac{\partial \phi_j}{\partial z}\right|_{z=h} = 0. \tag{8.48b}$$

In other words, ϕ_j are chosen as the eigenfunctions of the diffusion operator (8.48a), with ϱ_j as the eigenvalues. Multiplication of Eq. (8.48a) by ϕ_i and subsequent integration by parts in the left-hand side and use of the boundary conditions (8.48b) yield

$$\int_0^h \nu_{\mathrm{E}}\,\frac{\mathrm{d}\phi_i}{\mathrm{d}z}\,\frac{\mathrm{d}\phi_j}{\mathrm{d}z}\,\mathrm{d}z = \varrho_j \int_0^h \phi_i \phi_j\,\mathrm{d}z. \tag{8.49}$$

Note that for $i = j$, this relationship proves the eigenvalues to be positive for positive diffusion coefficients, since all other terms involved are quadratic and thus positive. Switching the indices i and j, we also have

$$\int_0^h \nu_{\mathrm{E}}\,\frac{\mathrm{d}\phi_j}{\mathrm{d}z}\,\frac{\mathrm{d}\phi_i}{\mathrm{d}z}\,dz = \varrho_i \int_0^h \phi_j \phi_i\,\mathrm{d}z, \tag{8.50}$$

and subtracting this equation from the preceding one, we obtain

$$(\varrho_i - \varrho_j) \int_0^h \phi_i \phi_j \, \mathrm{d}z = 0, \tag{8.51}$$

showing that for nonequal eigenvalues, the basis functions ϕ_i and ϕ_j are orthogonal in the sense that

$$\int_0^h \phi_i(z)\, \phi_j(z)\, \mathrm{d}z = 0 \quad \text{if} \quad i \neq j. \tag{8.52}$$

Finally, since the basis functions are defined within an arbitrary multiplicative factor, we may normalize them such that

$$\int_0^h \phi_i(z)\, \phi_j(z)\, \mathrm{d}z = \delta_{ij} = \begin{cases} 0 & \text{if } i \neq j \\ 1 & \text{if } i = j \end{cases} \tag{8.53}$$

When eigenfunctions are used as basis functions in the Galerkin method, a so-called *spectral method* is obtained. It is a very elegant method because the equations for the coefficients are greatly reduced. The orthonormality (8.53) of the eigenfunctions yields $\mathbf{M} = \mathbf{I}$, the identity matrix, and Eq. (8.49) in matrix form reduces to $\mathbf{K} = \boldsymbol{\varrho}\,\mathbf{M} = \boldsymbol{\varrho}$, where $\boldsymbol{\varrho}$ is a diagonal matrix formed with the eigenvalues ϱ_j. Finally, the equations for components j of $\mathbf{a}$ and $\mathbf{b}$ become

$$\frac{\mathrm{d}a_j}{\mathrm{d}t} = +f\, b_j - \varrho_j a_j - \frac{1}{\rho_0}\frac{\partial p}{\partial x} s_j + \frac{\tau^x}{\rho_0}\phi_j(h), \tag{8.54a}$$

$$\frac{\mathrm{d}b_j}{\mathrm{d}t} = -f\, a_j - \varrho_j b_j - \frac{1}{\rho_0}\frac{\partial p}{\partial y} s_j + \frac{\tau^y}{\rho_0}\phi_j(h). \tag{8.54b}$$

Note that, since the eigenvalues are positive, the second term on the right corresponds to a damping of the amplitudes a_j and b_j, consistent with physical damping by diffusion.

Because of the decoupling[7] achieved by a set of orthogonal basis functions, we no longer solve a system of $2N$ equations but N systems of 2 equations. This leads to a significant reduction in the number of operations to be performed: The standard Galerkin method requires, at every time step, one inversion of a matrix of size $2N \times 2N$ and a matrix multiplication of cost $4N^2$, whereas the spectral method demands solving N times a 2×2 system, with cost proportional to N. For a large number of time steps, the computational burden is roughly reduced by a factor N. With typically $10^2 - 10^3$ basis functions retained, the savings are

[7] Only when equations are linear.

very significant, and the use of a spectral method generates important gains in computing time. It is well worth the preliminary search of eigenfunctions.

In principle, for well-behaved $\nu_E(z)$, there exist an infinite but countable number of eigenvalues ϱ_j, and the full set of eigenfunctions ϕ_j allows the decomposition of any function. An approximate solution can thus be obtained by retaining only a finite number of eigenfunctions, and the questions that naturally come to mind are how many functions should be retained and which ones. To know which to retain, we can assume a constant viscosity ν_E, in which case the solution to the eigenproblem is (for $j=1,2,\ldots$)

$$\phi_j = \sqrt{\frac{2}{h}} \sin\left[(2j-1)\frac{\pi}{2}\frac{z}{h}\right]$$

$$\varrho_j = (2j-1)^2 \frac{\pi^2 \nu_E}{4h^2}$$

$$s_j = \frac{2\sqrt{2h}}{\pi(2j-1)}$$

$$\phi_j(h) = (-1)^{(j+1)}\sqrt{\frac{2}{h}}$$

in which the scaling factor $\sqrt{2/h}$ was introduced to satisfy the normalization requirement (8.53). The name *spectral method* is now readily understood in view of the type of eigenfunctions used in the expansion. The sine functions are indeed nothing else than those used in Fourier series to decompose periodic functions into different wavelengths. The coefficients a_j and b_j are directly interpretable in terms of modal amplitudes or, in other words, the energy associated with the corresponding Fourier modes. The sets of a_j and b_j then provide an insight into the spectrum of the solution.

We further observe that, the larger the eigenvalue ϱ_j, the more rapidly the function oscillates in space, allowing the capture of finer structures. Thus, a higher resolution is achieved by retaining more eigenfunctions in the expansion, just as adding grid points in finite differencing is done to obtain higher resolution. The number N of functions being retained is a matter of scales to be resolved. For a finite-difference representation with N degrees of freedom, the domain is covered with a uniform grid with spacing $\Delta z = h/N$, and the shortest scale that can be resolved has wavenumber $k_z = \pi/\Delta z$ (see Section 1.12). In the spectral method, the highest mode retained corresponds to wavenumber $k_z = N\pi/h$, which is identical to the one resolved in the finite-difference approach. Both methods are thus able to represent the same spectrum of wavenumbers with an identical number of unknowns. Also, the cost of both methods is directly proportional to the number of unknowns. So, where is the advantage of using a spectral method?

Except for the straightforward interpretation of the coefficients a_j and b_j in terms of Fourier components, the essential advantage of spectral methods

resides in their rapid convergence as the number N of basis functions is increased, for sufficiently gentle solutions and boundary conditions (e.g., Canuto, Hussaini, Quarteroni & Zang, 1988). To illustrate this claim, we calculate the stationary solution of a geostrophic current without surface stress by dropping $\mathrm{d}a_j/\mathrm{d}t$ and $\mathrm{d}b_j/\mathrm{d}t$ from the matrix equations and solve for $\mathbf{a}$ and $\mathbf{b}$ before recombining the solution. Even with only five basis functions (i.e., equivalent to using five grid points), the behavior of the solution is well captured (Fig. 8.12). Furthermore, since the equations for different a_j coefficients are decoupled, increasing the value of N does not modify the values of the previously calculated coefficients but simply adds more terms, each one bringing additional resolution. The amplitude of the new terms is directly proportional to the value of the coefficients a_j and b_j, and their rapid decrease as a function of index j (Fig. 8.13—note the logarithmic scales) explains why fast convergence can be expected.

In order not to miss the most important parts of the solution, it is imperative to use eigenfunctions in their order, that is, without skipping any in the series, up to the preselected number N. In the limit of large N, it can be shown

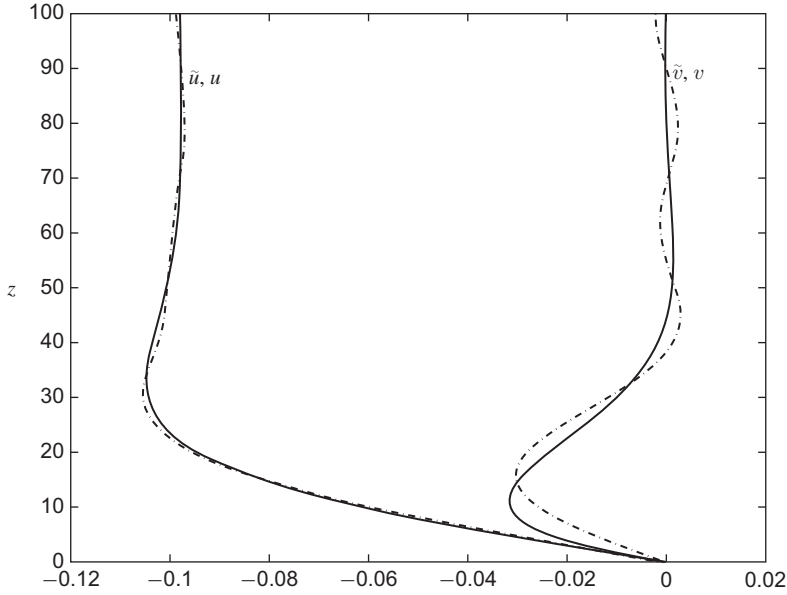

FIGURE 8.12 Velocity profile forced by a pressure gradient directed along the y-axis above a no-slip bottom and below a stress-free surface. The geostrophic flow aloft has components $u = 0.1$ and $v = 0$. Solid lines represent the exact solution, whereas dash-dotted lines depict the numerical solution obtained by the spectral method with only the first five modes. Note the excellent agreement. Oscillations appearing in the numerical solution give a hint of the sine functions used in expanding the solution.

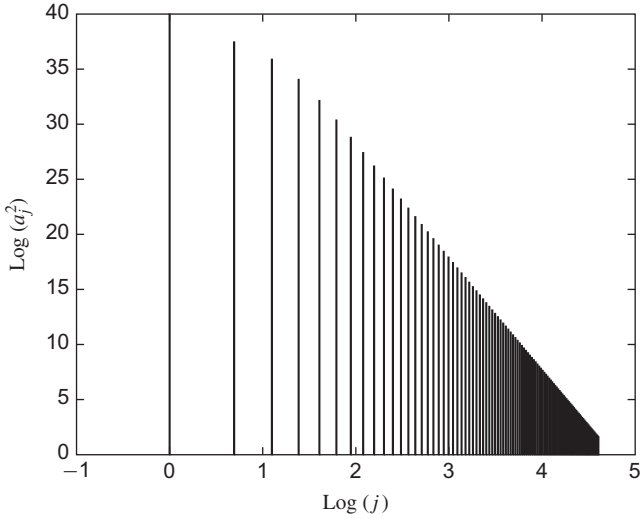

FIGURE 8.13 Sequential values of the coefficients a_j (scaled by an arbitrary coefficient) obtained with the spectral method applied to the problem of Fig. 8.12. Scales are logarithmic, showing the rapid decrease of amplitudes with increasing number of modes in the expansion. Convergence toward the exact solution is fast.

that convergence for a relatively smooth solution is faster than with any finite-difference method of any order (e.g., Gottlieb & Orszag, 1977). This is the distinct advantage of the spectral method, which explains why it is often used in cases when nearly exact numerical solutions are sought.

An alternative to the Galerkin spectral approach is to force the error to vanish at particular grid points, leading to so-called *pseudospectral methods* (e.g., Fornberg, 1988). As for all collocation methods, these do not require evaluation of integrals over the domain.

In concluding the presentation of the function-expansion approach, we insist on the fundamental aspect that the numerical approximation is very different from the point-value sampling used in finite-difference methods. In space, the basis functions ϕ_j are continuous and can therefore be differentiated or manipulated mathematically without approximation. The numerical error arises only due to the fact that a finite number of basis functions is used to represent the solution.

ANALYTICAL PROBLEMS

8.1. It is observed that fragments of tea leaves at the bottom of a stirred tea cup conglomerate toward the center. Explain this phenomenon with Ekman-layer dynamics. Also explain why the tea leaves go to the center irrespectively of the direction of stirring (clockwise or counterclockwise).

8.2. Assume that the atmospheric Ekman layer over the Earth's surface at latitude 45°N can be modeled with an eddy viscosity $\nu_E = 10$ m^2/s. If the geostrophic velocity above the layer is 10 m/s and uniform, what is the vertically integrated flow across the isobars (pressure contours)? Is there any vertical velocity?

8.3. Meteorological observations above New York (41°N) reveal a neutral atmospheric boundary layer (no convection and no stratification) and a westerly geostrophic wind of 12 m/s at 1000 m above street level. Under neutral conditions, Ekman dynamics apply. Using an eddy viscosity of 10 m^2/s, determine the wind speed and direction atop the Empire State Building, which stands 381 m tall.

8.4. A southerly wind blows at 9 m/s over Taipei (25°N). Assuming neutral atmospheric conditions so that Ekman dynamics apply and taking the eddy viscosity equal to 10 m^2/s, determine the velocity profile from street level to the top of the 509 m tall Taipei Financial Center skyscraper. The wind force per unit height and in the direction of the wind can be taken as $F = 0.93\rho LV^2$, where ρ = 1.20 kg/m^3 is the standard air density, L = 25 m is the building width, and $V(z) = (u^2 + v^2)^{1/2}$ is the wind speed at the height considered. With this, determine the total wind force on the southern facade of the Taipei Financial Center.

8.5. Show that although $\bar{w}$ may not be zero in the presence of horizontal gradients, the vertical advection terms $w\partial u/\partial z$ and $w\partial v/\partial z$ of the momentum equations are still negligible, even if the short distance d is taken as the vertical length scale.

8.6. You are working for a company that plans to deposit high-level radioactive wastes on the bottom of the ocean, at a depth of 3000 m. This site (latitude: 33°N) is known to be at the center of a permanent counterclockwise vortex. Locally, the vortex flow can be assimilated to a solid-body rotation with angular speed equal to 10^{-5} s^{-1}. Assuming a homogeneous ocean and a steady, geostrophic flow, estimate the upwelling rate at the vortex center. How many years will it take for the radioactive wastes to arrive at the surface? Take $f = 8 \times 10^{-5}$ s^{-1} and $\nu_E = 10^{-2}$ m^2/s.

8.7. Derive Eq. (8.36) more simply not by starting from solution (8.33) as done in the text but by vertical integration of the momentum equations (8.32). Consider also the case of nonuniform eddy viscosity, in which case ν_E must be kept inside the vertical derivative on the right-hand side of the equations, as in the original governing equations (4.21a) and (4.21b).

8.8. Between 15°N and 45°N, the winds over the North Pacific Ocean consist mostly of the easterly trades (15°N to 30°N) and the midlatitude

westerlies (30°N to 45°N). An adequate representation is

$$\tau^x = \tau_0 \sin\left(\frac{\pi y}{2L}\right), \qquad \tau^y = 0 \quad \text{for} \quad -L \le y \le L,$$

with $\tau_0 = 0.15$ N/m^2 (maximum wind stress) and $L = 1670$ km. Taking $\rho_0 = 1028$ kg/m^3 and the value of the Coriolis parameter corresponding to 30°N, calculate the Ekman pumping. Which way is it directed? Calculate the vertical volume flux over the entire 15°–45°N strip of the North Pacific (width = 8700 km). Express your answer in sverdrup units (1 sverdrup = 1 Sv = 10^6 m^3/s).

8.9. The variation of the Coriolis parameter with latitude can be approximated as $f = f_0 + \beta_0 y$, where y is the northward coordinate (beta-plane approximation, see Section 9.4). Using this, show that the vertical velocity below the surface Ekman layer of the ocean is given by

$$\bar{w}(z) = \frac{1}{\rho_0}\left[\frac{\partial}{\partial x}\left(\frac{\tau^y}{f}\right) - \frac{\partial}{\partial y}\left(\frac{\tau^x}{f}\right)\right] - \frac{\beta_0}{f}\int_z^0 \bar{v}\,\mathrm{d}z, \tag{8.55}$$

where τ^x and τ^y are the zonal and meridional wind-stress components, respectively, and $\bar{v}$ is the meridional velocity in the geostrophic interior below the Ekman layer.

8.10. Determine the vertical distribution of horizontal velocity in a 4-m deep lagoon subject to a northerly wind stress of 0.2 N/m^2. The density of the brackish water in the lagoon is 1020 kg/m^3. Take $f = 10^{-4}$ s^{-1} and $\nu_E = 10^{-2}$ m^2/s. In which direction is the net transport in this brackish layer?

8.11. Redo Problem 8.10 with $f = 0$ and compare the two solutions. What can you conclude about the role of the Coriolis force in this case?

8.12. Find the stationary solution of (8.13a)–(8.13c) for constant viscosity, a uniform pressure gradient in the y-direction in a domain of finite depth h with no stress at the top and no slip at the bottom. Study the behavior of the solution as h/d varies and compare with the solution in the infinite domain. Then, derive the stationary solution without pressure gradient but with a top stress in the y-direction.

NUMERICAL EXERCISES

8.1. How can we obtain initial conditions for a_j and b_j in the expansions (8.40) from initial conditions on the physical variables $u = u_0(z)$ and $v = v_0(z)$?

(*Hint*: Investigate a least-square approach and an approach in which the initial error is forced to vanish in the sense of Eq. (8.42). When do the two approaches lead to the same result?)

8.2. Use `spectralekman.m` to calculate numerically the stationary solutions of Analytical Problem 8.12. Compare the exact and numerical solutions for $h/d = 4$ and assess the convergence rate as a function of $1/N$, where N is the number of eigenfunctions retained in the trial solution. Compare the convergence rate of both cases (with and without stress at the top) and comment.

8.3. Use `spectralekman.m` to explore how the solution changes as a function of the ratio h/d and how the number N of modes affects your resolution of the boundary layers.

8.4. Modify `spectralekman.m` to allow for time evolution, but maintaining constant wind stress and pressure gradient. Use a trapezoidal method for time integration. Start from rest and observe the temporal evolution. What do you observe?

8.5. Use a finite-volume approach with time splitting for the Coriolis terms and an explicit Euler method to discretize diffusion in Eqs. (8.39a) and (8.39b). Verify your program in the case of uniform eddy viscosity by comparing with the steady analytical solution. Then, use the viscosity profile $\nu_E(z) = \mathcal{K}z(1 - z/h)u_*$. In this case, can you find the eigenfunctions of the diffusion operator and outline the Galerkin method? (*Hint*: Look for Legendre polynomials and their properties.)

8.6. Assume that your vertical grid spacing in a finite-difference scheme is large compared with the roughness length z_0 and that your first point for velocity calculation is found at the distance $\Delta z/2$ above the bottom. Use the logarithmic profile to deduce the bottom stress as a function of the computed velocity at level $\Delta z/2$. Then, use this expression in the finite-volume approach of Numerical Exercise 8.5 to replace the no-slip condition by a stress condition at the lowest level of the grid.

Vagn Walfrid Ekman
1874–1954

Born in Sweden, Ekman spent his formative years under the tutelage of Vilhelm Bjerknes and Fridtjof Nansen in Norway. One day, Nansen asked Bjerknes to let one of his students make a theoretical study of the influence of the earth's rotation on wind-driven currents, on the basis of Nansen's observations during his polar expedition that ice drifts with ocean currents to the right of the wind. Ekman was chosen and later presented a solution in his doctoral thesis of 1902.

As professor of mechanics and mathematical physics at the University of Lund in Sweden, Ekman became the most famous oceanographer of his generation. The distinguished theoretician also proved to be a skilled experimentalist. He designed a current meter, which bears his name and which has been used extensively. Ekman was also the one who explained the phenomenon of dead water by a celebrated laboratory experiment (see Fig. 1.4). (*Photo courtesy of Pierre Welander*)

Ludwig Prandtl
1875–1953

A German engineer, Ludwig Prandtl was attracted by fluid phenomena and their mathematical representation. He became professor of mechanics at the University of Hannover in 1901, where he established a world renowned institute for aerodynamics and hydrodynamics. It was while working on wing theory in 1904 and studying friction drag in particular that he developed the concept of boundary layers and the attending mathematical technique. His central idea was to recognize that frictional effects are confined to a thin layer in the vicinity of the boundary, allowing the modeler to treat rest of the flow as inviscid.

Prandtl also made noteworthy advances in the study of elasticity, supersonic flows, and turbulence, particularly shear turbulence in the vicinity of a boundary. A mixing length and a dimensionless ratio are named after him.

It has been remarked that Prandtl's keen perception of physical phenomena was balanced by a limited mathematical ability and that this shortcoming prompted him to seek ways of reducing the mathematical description of his objects of study. Thus perhaps, the boundary-layer technique was an invention born out of necessity. (*Photo courtesy of the Emilio Segrè Visual Archives, American Institute of Physics*)